A Universal Urbach Rule for Disordered Organic Semiconductors

Christina Kaiser
Swansea University
Oskar Sandberg
Swansea University
Nasim Zarrabi
Swansea University
Wei Li
Swansea University
Paul Meredith
Swansea University https://orcid.org/0000-0002-9049-7414
Ardalan Armin (ardalan.armin@swansea.ac.uk)
Swansea University https://orcid.org/0000-0002-6129-5354

Article

Keywords:

Posted Date: February 24th, 2021

DOI: https://doi.org/10.21203/rs.3.rs-106584/v1

Version of Record: A version of this preprint was published at Nature Communications on June 28th, 2021. See the published version at https://doi.org/10.1038/s41467-021-24202-9.

A Universal Urbach Rule for Disordered Organic Semiconductors

Christina Kaiser, Oskar J. Sandberg*, Nasim Zarrabi, Wei Li, Paul Meredith, Ardalan Armin*

Sustainable Advanced Materials (Sêr-SAM), Department of Physics, Swansea University, Singleton Park, Swansea SA2 8PP, United Kingdom

*Email: ardalan.armin@swansea.ac.uk; o.j.sandberg@swansea.ac.uk

Abstract

In crystalline semiconductors, the sharpness of the absorption spectrum onset is characterized by temperature-dependent Urbach energies. These energies quantify the static, structural disorder causing localized exponential tail states, and the dynamic disorder due to electron-phonon scattering. The applicability of this exponential-tail model to molecular and amorphous solids has long been debated. Nonetheless, exponential fittings are routinely applied to the analysis of the sub-gap absorption of organic semiconductors alongside Gaussian-like spectral line-shapes predicted by non-adiabatic Marcus theory. Herein, we elucidate the sub-gap spectral line-shapes of organic semiconductors and their blends by temperature-dependent quantum efficiency measurements in photovoltaic structures. We find that the Urbach energy associated with singlet excitons universally equals the thermal energy regardless of static disorder. These observations are consistent with absorption spectra obtained from a convolution of Gaussian density of excitonic states weighted by a Boltzmann factor. A generalized Marcus charge transfer model is presented that explains the absorption spectral line-shape of disordered molecular matrices, and we also provide a simple strategy to determine the excitonic disorder energy. Our findings elaborate the true meaning of the dynamic Urbach energy in molecular solids and deliver a way of relating the photo-physics to static disorder, crucial for optimizing molecular electronic devices such as organic solar cells.

Introduction

Recently, research on organic solar cells has seen significant progress through the development of non-fullerene electron acceptors (or NFAs), in particular delivering increases in single-junction efficiencies from 13.1 to 17.3 % between 2018 to 2020.[1,2] This has revived ambitions to ultimately achieve industrial scale low-cost photovoltaics with low embodied manufacturing energy. While chemists have been productively synthesising new materials, understanding of the opto-electronic properties lags behind – particularly in relation as to why these new n-type organic semiconductors are so effective at photogeneration with low voltage losses. A particular area of intense interest is light absorption and how it is related to molecular dipole moments and their energetic disorder. Of course, this is also a very relevant question for the fundamental solid state physics of molecular and disordered semiconductors.

In general, semiconductors tend to absorb light at photon energies below the bandgap (sub-gap absorption) depending on the energetic disorder. In the case of inorganic semiconductors, the absorption coefficient often displays an exponential tail below the bands. These so-called Urbach tails increase their broadening with temperature T.[3] The sub-gap absorption coefficient generally follows the expression

$$\alpha(E,T) \propto \exp\left(\frac{E-E_{\mathrm{on}}(T)}{E_{\mathrm{U}}(T)}\right), \quad (1)$$

where E is the photon energy and E_{on} is the energy onset of the tail correlated to the bandgap energy. E_{U} is the Urbach energy and it can vary between 10 to 100 meV depending on the semiconductor.[4–7] In banded semiconductors, the Urbach energy is believed to be related to the energetic disorder via $E_{\mathrm{U}}(T) = \sigma_{\mathrm{D}}(T) + \sigma_{\mathrm{S}}$. Here, $\sigma_{\mathrm{D}}(T)$ is a temperature-dependent dynamical disorder term related the thermal occupation of phonon states,[4,8] while σ_{S} is a temperature-independent term associated with structural or static disorder.[9] In this regard, σ_{S} is the standard deviation of the distribution of localized states (induced by structural disorder) below the band edges. However, a unifying theory describing the density of states and their absorption leading to Urbach tails for materials of different chemical bonding and morphology is still lacking.[10,11]

In amorphous (disordered) semiconductors, the definition of a clear bandgap edge is often difficult due to large σ_{S} inducing sub-gap broadening. Organic semiconductors, which are excitonic and partially amorphous, display even more complex sub-gap features including intermolecular hybrid charge transfer (CT) states in technologically-relevant blends of electron donors and acceptors (analogous to p-and-n-type semiconductors respectively)[12], excitonic features[13] and trap states[14]. CT and trap states give rise to light absorption with Gaussian sub-gap spectral line-shapes in accordance with non-adiabatic Marcus theory. The associated CT energy is often seen as an effective bandgap found to correlate with the open-circuit voltage.[12,15]

With the recent rise of non-fullerene electron-accepting semiconductors with small energetic offset relative to donors[16], the lack of CT state sub-gap spectral features in donor-acceptor blends has led to the increased usage of Urbach energies to understand disorder and sub-gap photo-physics. As a rule of thumb, it has been assumed that low Urbach energies are indicative of lower σ_{S} and hence expected to result in higher performance such as reduced charge recombination and higher charge carrier mobilities in a photovoltaic device.[17–19] Due to the complex and often convoluted spectral features in sub-gap light absorption of organic semiconductors, Urbach energy carries significant ambiguity. Moreover, a long-standing debate[20–22] on the distribution of density of states (DOS) defining σ_{S} in organic semiconductors has been revived: does the DOS follow a Gaussian or an exponential distribution? With no doubt, the origin of σ_{S} is of great importance for the classification

and future development of organic semiconductors and their electro-optical properties. However, it has remained unclear how this important figure-of-merit relates to the Urbach energy.

In this work, we show that the exciton sub-gap absorption in organic semiconductors is generally characterized by Urbach tails with characteristic energies equivalent to the thermal energy kT as demonstrated by temperature-dependent EQE measurements. However, these Urbach tails are often convoluted with Gaussian line-shapes induced by trap states and/or CT states, resulting in erroneous, energy-dependent, Urbach energies larger than kT. A simple model, combining the Gaussian distributed DOS with a Boltzmann factor for the absorption rate, is shown to reproduce the absorption profiles and to give an estimate for σ_{S}.

Results

The spectral line-shape of the absorption coefficient and the EQE in the sub-gap tail ($\alpha d \ll 1$) are generally related via a modified Beer-Lambert law, $\mathrm{EQE} = \tilde{f}\alpha d$, where d is the thickness of the active layer and $\tilde{f}$ is an energy-dependent correction factor accounting for optical interference.[23,24] Since $\tilde{f}$ is often assumed to be close to 1 for typical active thicknesses from 100 to 150 nm, EQE measurements have been used in the past to determine the Urbach energy, the EQE in this case following the spectral shape of α. A previous lack of sensitivity in the EQE measurements has led to speculative assumptions about the spectral range of trap state absorptions, exponential tails and associated Urbach energies in organic semiconductors. By choosing a small fitting range exponential fits can be forced on to EQE spectra resulting in rather arbitrary Urbach energies, dependent on the spectral range of the fitting. More insight is gained from the apparent Urbach energy ($E_{\mathrm{U}}^{\mathrm{app}}$) here defined as:

$$E_{\mathrm{U}}^{\mathrm{app}}(E) = \left[\frac{d\ln(\mathrm{EQE})}{dE}\right]^{-1} \tag{2}$$

For a true exponential tail of the form eq. 1, $E_{\mathrm{U}}^{\mathrm{app}}$ is constant in the sub-gap spectral region and given by $E_{\mathrm{U}}(T)$ under the assumption of negligible optical interference effects.

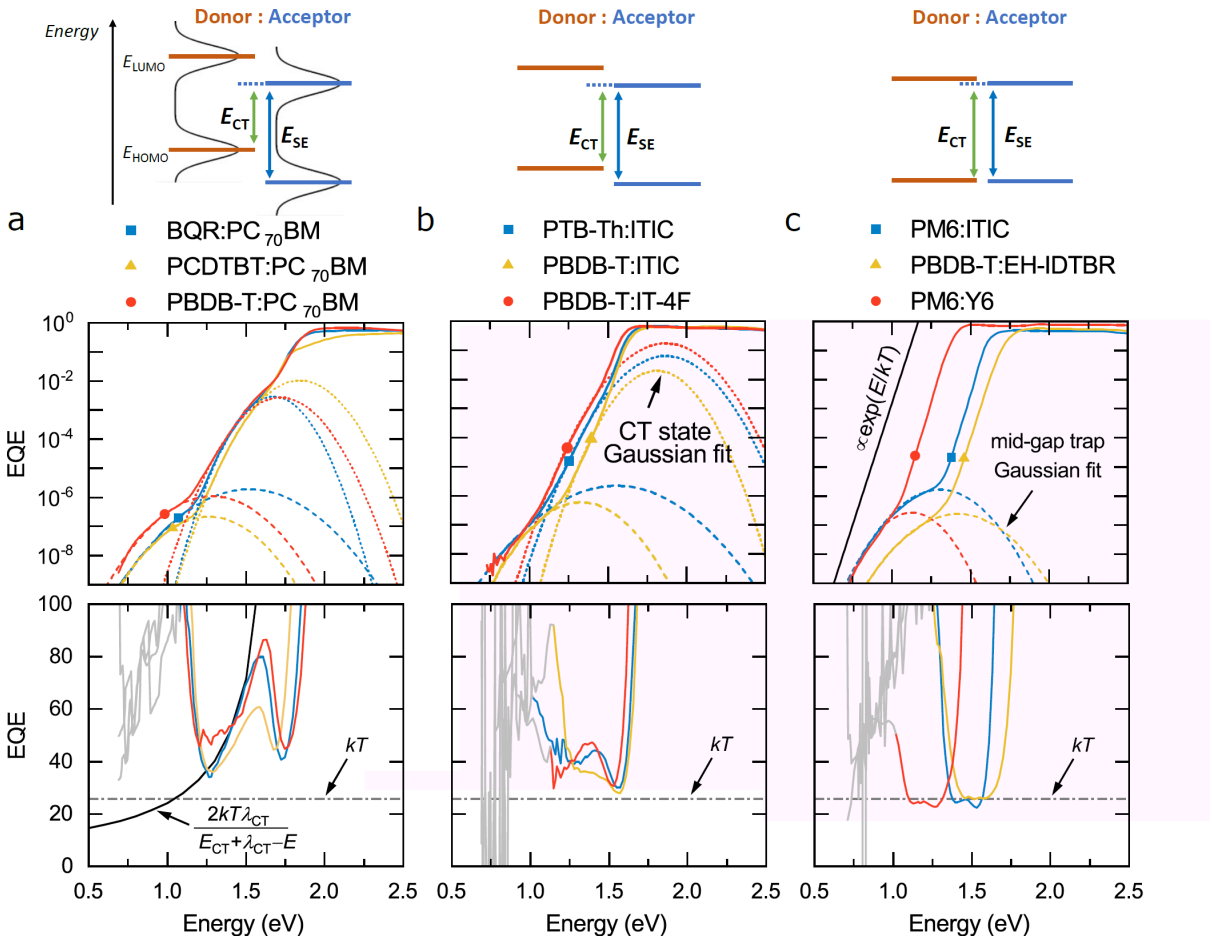

Figure 1 | EQE and E_U^{app} for organic BHJs with different energetic offsets between the HOMO energy levels of donor and acceptor. From Gaussian fits in the spectral range of charge transfer state and trap state absorption, the charge transfer energy (E_{CT}) and trap energy (E_t) are extracted where possible. For low-energy offset materials, such as PM6:Y6, PM6:ITIC and PBDB-T:EH-IDTBR, the EQE tail has the form $e^{E/kT}$ and E_U^{app} roughly equals kT in the spectral range that is dominated by the absorption of the acceptor. For large-offset material systems, such as BQR:$PC_{70}BM$, PBDB-T:$PC_{70}BM$ and PCDTBT:$PC_{70}BM$, E_U^{app} shows a $2kT\lambda_{CT}/(E_{CT}+\lambda_{CT}-E)$ dependence in the spectral range of CT absorption.

Figure 1 shows the EQE and E_U^{app} for a wide range of organic semiconductor donor-acceptor (DA) blends. The material systems studied here can be generally grouped according to the DA energy offset or, in other words, by the difference between the CT state energy E_{CT} and the optical gap of singlet excitons E_{SE}, as illustrated in Figure 1. Large offset systems, such as PCDTBT:$PC_{70}BM$, BQR:$PC_{70}BM$ and PBDB-T:$PC_{70}BM$, show three distinct spectral ranges for energies below the gap: (i) mid-gap trap state absorption at energies below 1.2 eV, (ii) CT state absorption in the mid-range (~1.2 – 1.5 eV) and (iii) SE absorption above 1.5 eV. For mid-gap and CT state absorption, Gaussian-shaped EQE features are observed.[14] These features are consistent with Marcus charge-transfer between states that are distributed in accordance with a Gaussian density of sub-gap states. The associated absorption coefficients are $\alpha_{CT}(E) = g(E, E_{CT}, \lambda_{CT}, f_{CT})$ and $\alpha_t(E) = g(E, E_t, \lambda_t, f_t)$ for CT and mid-gap state absorption, respectively, where

$$g(E, E_j, \lambda_j, f_j) = f_j E^{-1} (4\pi\lambda_j kT)^{-\frac{1}{2}} \exp\left(-\frac{(E_j + \lambda_j - E)^2}{4\lambda_j kT}\right). \quad (3)$$

Here, f_j is a prefactor that depends on the oscillator strength and number density of states, whereas E_j and λ_j are the energy and reorganization energy of the states, respectively, both being generally dependent of the width of the Gaussian DOS (see **Supplementary Information**). The fit parameters obtained for this work are summarized in **Table S1.** As highlighted by the black solid line in Figure 1, E_U^{app} in the spectral range of CT absorption is strongly energy-dependent and closely follows $E_U^{app} \approx 2kT\lambda_{CT}/(E_{CT} + \lambda_{CT} - E)$ as expected from eq. 3. At higher energies corresponding to sub-gap SE absorption, E_U^{app} has a narrow parabolic shape with a sharp minimum at roughly 40 - 50 meV for the large offset blends.

The EQE and E_U^{app} of blends with a smaller offset between E_{CT} and E_{SE} (PTB7-Th:ITIC, PBDB-T:ITIC and PBDB-T:IT-4F) are shown in the middle panel of Figure 1. In this case, the Gaussian CT state line-shape is barely recognizable, and the SE absorption tail of the acceptor is visible over a wider spectral range. While E_U^{app} retains its parabolic shape in the SE absorption regime, because of the wider range, the minimum value of E_U^{app} is significantly reduced to values close to kT. Finally, the EQE and E_U^{app} of blends in low-offset systems (PM6:Y6, PM6:ITIC and PBDB-T:EH-IDTBR) are shown in the right panel of Figure 1. Such systems are characterized by similar energies for the highest occupied molecular orbital (HOMO) of the donor and the HOMO of the acceptor as illustrated in Figure 1. In these blends, the CT state absorption can no longer be discerned from the EQE spectra. Instead, the SE absorption remains dominant down to the energy range of mid-gap state excitation. In this limit, the E_U^{app} in the SE-dominated range finally saturates and reaches a broad plateau where $E_U^{app} \approx kT$.

The above experimental observation for low-offset D-NFA systems (where $E_{CT} \approx E_{SE}$) suggests that intramolecular sup-gap absorption may generally follow $\alpha \propto \exp(E/kT)$, but that its spectroscopic observation is obstructed by CT absorption in systems with larger offsets. To further clarify this, systems where one absorbing species dominates the sub-gap EQE spectrum were investigated and the data shown in **Figure 2**. In the case of neat $PC_{70}BM$ (Figure 2a), a narrow spectral range where $E_U^{app} \approx kT$ can be identified. The spectral range is limited by trap-state absorption at low energies, while at high energies poor exciton dissociation severely reduces the EQE. However, the range can be increased by adding 0.1 mol% of the wide-gap donor m-MTDATA, resulting in enhanced exciton dissociation (we note that in this case the fullerene acceptor is the narrower gap component). Since m-MTDATA:$PC_{70}BM$ is characterized by a low E_{CT}, the singlet exciton tail from $PC_{70}BM$ can be clearly distinguished from CT states as shown in Figure 2a.[26] By further increasing the donor content, the CT state absorption increases and the parabolic shape of E_U^{app} emerges. This explains the parabolic shapes, seen for systems where $E_{CT} \ll E_{SE}$ in Figure 1, which appear when the SE absorption regime with $E_U^{app} \approx kT$ becomes convoluted with CT state absorption. This is further supported by results for neat NFA devices comprising ITIC and IT-4F active layers, respectively, with the SE tail of the acceptor again following an inverse slope of kT, as shown in Figure 2b.

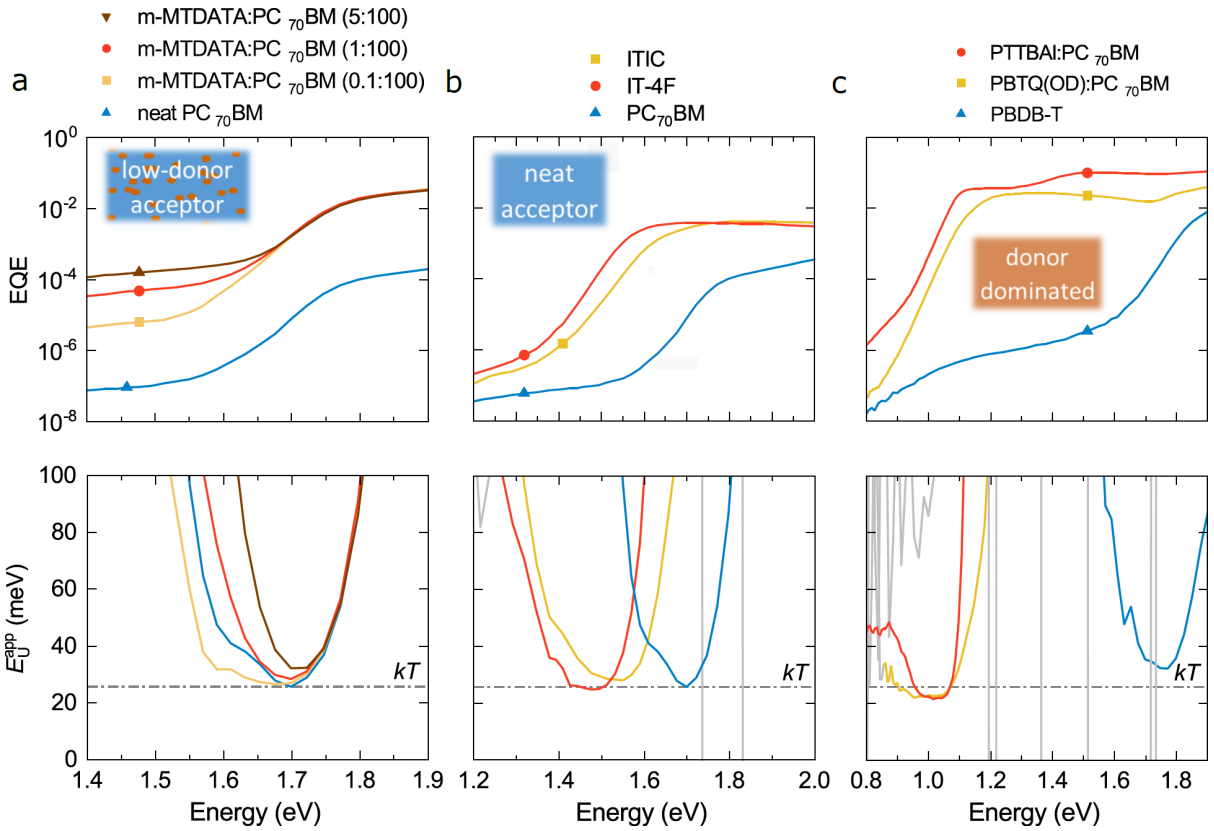

Figure 2 | EQE tail dominated by neat material absorption. a, The inverse slope of the logarithm of the EQE for a series of m-MTDATA sensitized $PC_{70}BM$ solar cells. The widest energy range over which E_U^{app} equals kT is observed for 0.1 mol% m-MTDATA in $PC_{70}BM$ due to improved exciton dissociation in comparison to neat $PC_{70}BM$. BHJ examples for which the EQE tail is partially dominated by **b,** the neat donor absorption or by **c,** the neat acceptor absorption hence showing $E_U^{app} \approx kT$ in some parts of the spectrum. EQE spectra of PTTBAI:$PC_{70}BM$ and PBTQ(OD):$PC_{70}BM$ are taken from reference 27.

To check if $E_U^{app} \approx kT$ is also true for donor materials has proven more challenging, since the neat donor absorption is often convoluted with deep trap-state absorption, effectively increasing E_U^{app} above kT as shown for PBDB-T in Figure 2c, where $E_U^{app} \approx 30$ meV. This problem can be circumvented by using narrow-gap polymer donors such as PBTQ(OD) or PTTBAI, which show strongly redshifted EQE spectra when blended with $PC_{70}BM$ as previously reported.[27] As shown in Figure 2c, E_U^{app} is around 22 meV in this case. While deviations of the type $E_U^{app} > kT + 10$ meV are due to the presence of other absorbing species like CT states or deep trap states, small deviations of E_U^{app} around kT are likely caused by interference effects, i.e. non-constant $\tilde{f}$, as shown previously.[23,28] Interference effects arises from the spectral dependence of the optical constants of the different layers in the thin-film stack and generally vary with the thickness of the active layer. To demonstrate the presence of interference effects, we therefore fabricated PM6:ITIC devices and PM6:Y6 devices of different active layer thicknesses. Indeed, as illustrated in the **Figures S3**, E_U^{app} shows a weak thickness dependence leading to deviations around kT from $+2.3$ meV to -5.8 meV. The thickness dependence of E_U^{app} is further corroborated by optical transfer-matrix simulations (see **Figure S4** in the **Supplementary Information**).

To verify that the absorption coefficient tail of the excitons follows a Boltzmann factor, we performed T-dependent EQE measurements on PBDB-T:EH-IDTBR, PM6:Y6 and PM6:ITIC, and the neat materials IT-4F and Y6. **Figure 3a** shows the normalized EQE and the respective $E_{\mathrm{U}}^{\mathrm{app}}$ spectra of three representative systems: PBDB-T:EH-IDTBR, PM6:Y6 and IT-4F. The remaining material systems are provided in the **Supplementary Information**. Depending on T, two different regimes can be distinguished in the sub-gap absorption tail: At high T, $E_{\mathrm{U}}^{\mathrm{app}}$spectra show a T-dependent plateau only influenced by interference effects and the shift in the absorption onset. At low T, however, the $E_{\mathrm{U}}^{\mathrm{app}}$spectra generally attain a parabolic shape suggesting that the SE tail becomes convoluted with CT and/or mid-gap states. The thermal activation of the excitonic absorption tail is then finally illustrated by plotting the local minimum of $E_{\mathrm{U}}^{\mathrm{app}}$ (denoted as min($E_{\mathrm{U}}^{\mathrm{app}}$) in **Figure 3b**) in the plateau region as a function of kT for all systems studied. We see that min($E_{\mathrm{U}}^{\mathrm{app}}$) at higher temperature is linear and equals kT + constant, where the constant offset arises from interference effects. At lower T, min($E_{\mathrm{U}}^{\mathrm{app}}$) eventually deviates from linearity, as the spectral shape is increasingly affected by other absorbing species. For example, the low-energy tail of the CT absorption may emerge at low T owing to its distinctly different T-dependence compared to SE. Moreover, the absorption of trap states is expected to play a role as well, while little is yet known about their spectral broadening as a function of T.

For comparison, we also measured T-dependent EQE spectra of a commercial a-Si:H thin-film solar cell (EQE and $E_{\mathrm{U}}^{\mathrm{app}}$ spectra shown in **Figure S6**). In banded semiconductors such as a-Si:H, the total energetic disorder is $E_{\mathrm{U}}(T) = \sigma_{\mathrm{s}} + \sigma_{\mathrm{D}}(T)$, where $\sigma_{\mathrm{D}}(T)$ is often described by the Einstein solid model as the thermal occupation of phonon modes.[4] In **Figure 3b**, two regimes can be distinguished for a-Si:H: the low temperature saturation of min($E_{\mathrm{U}}^{\mathrm{app}}$) to $E_{\mathrm{U}}(0) = 38$ meV and thermal activation at higher temperatures with an offset of roughly 16 meV from kT, in agreement with previous reports.[25,29,30] In contrast, for the organic semiconductor systems in **Figure 3b**, an extrapolation to $T = 0$ results in $\sigma_{\mathrm{s}} \approx 0$, suggesting that the Urbach energy is not governed by static disorder in these systems. This raises the question why excitons in organic semiconductors follow a Boltzmann factor resulting in $E_{\mathrm{U}}^{\mathrm{app}} \approx kT$ and what is the role of σ_{s} in shaping the $E_{\mathrm{U}}^{\mathrm{app}}$ spectra. Answering this question may be a key to understanding the light-matter interaction in these systems.

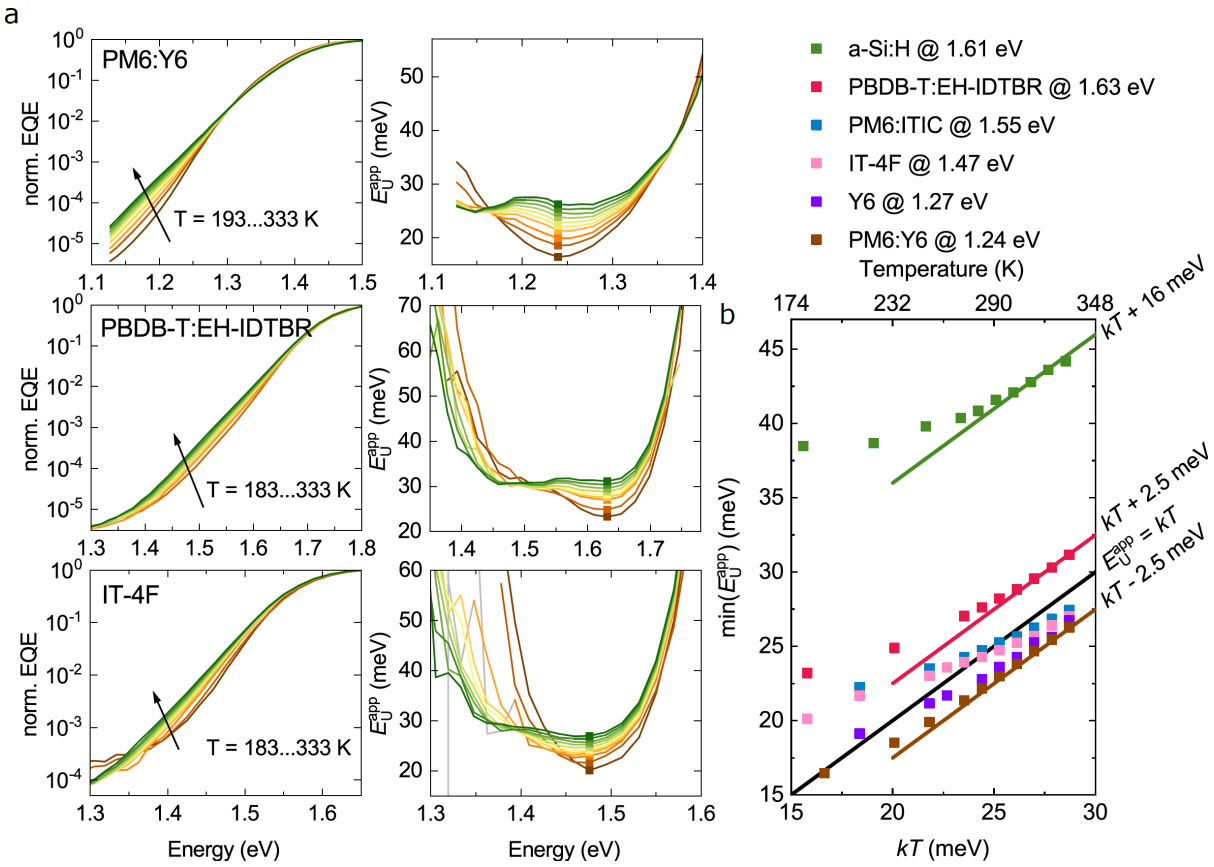

Figure 3 | Temperature dependent apparent Urbach energies. a, Normalized sub-gap EQE and Urbach energy (E_U^{app}) spectra of inverted PM6:Y6, PBDB-T:EH-IDTBR and neat IT-4F solar cells at different temperatures. Independent of temperature, E_U^{app} spectra show a local minimum (solid markers) at a constant energy within the spectral range dominated by exciton absorption. **b,** Minimum E_U^{app} as a function of kT for all tested materials systems including a commercial a-Si:H thin-film solar cell.

In the context of the Marcus formalism for non-adiabatic charge transfer (high-temperature limit), $E_U^{app} \approx kT$ in the spectral range of SE absorption may be rationalized in terms of non-equal potential energy surfaces for the SE state and the ground state. By assuming a significantly more diffuse or delocalized SE state, compared to the (strongly localized) ground state, a much smaller reorganization energy is obtained for the SE excited state in comparison to the ground state.[31–33] In this limit, we expect $\alpha_{SE}(E, E_{SE}) \approx \alpha_{sat} \exp([E - E_{SE}]/kT)$ for $E < E_{SE}$, where E_{SE} is the energy of the singlet state (see **Supplementary Information**). Here, α_{sat} includes a $1/E$ dependence, however, the sub-gap spectral line-shape is dominated by the Boltzmann factor. For above-gap absorption, we assume $\alpha_{SE}(E, E_{SE}) \approx \alpha_{sat}$ for $E > E_{SE}$. We note that this simplification of $\alpha_{SE}(E, E_{SE})$ essentially follows a Miller-Abrahams-type charge-transfer formalism, sometimes used to describe exciton migration[34], but more commonly used for charge transport[35] in organic semiconductors. Accounting for a DOS given by $g_{DOS}(E_{SE})$, the total absorption coefficient is of the form $\alpha_{SE}(E) = \int \alpha_{SE}(E, E_{SE}) g_{DOS}(E_{SE}) dE_{SE}$. In the **Supplementary Information**, expressions for the associated absorption coefficient are derived for the cases of a Gaussian DOS and an exponential tail DOS. For the case of an exponential tail DOS with the width W, we obtain $E_U^{app} = W$ (see **Figure S7**). This is indeed not what we observe in experiments. For a Gaussian DOS, in turn, we obtain an absorption coefficient of the form

$$\frac{\alpha(E)}{\alpha_{\mathrm{sat}}} = \exp\left(\frac{E - E_{SE,0} + \frac{\sigma_s^2}{2kT}}{kT}\right)\left[1 - \mathrm{erf}\left(\frac{E - E_{SE,0} + \frac{\sigma_s^2}{kT}}{\sigma_s\sqrt{2}}\right)\right] + \mathrm{erf}\left(\frac{E - E_{SE,0}}{\sigma_s\sqrt{2}}\right) + 1 \quad (4)$$

where σ_s is the standard deviation of the Gaussian DOS and $E_{\mathrm{SE},0}$ is the DOS centre, i.e. the mean exciton energy. For $E \ll E_{\mathrm{SE},0}$, eq. 4 reduces to the exponential part and $E_{\mathrm{U}}^{\mathrm{app}}$ therefore equals kT. For $E \geq E_{\mathrm{SE},0}$, the error functions (with $\sigma_s\sqrt{2}$ in the denominator) govern the spectral shape at the absorption edge as demonstrated in **Figure S8** in the **Supplementary Information**.

The above model explains the observed $E_{\mathrm{U}}^{\mathrm{app}} = kT$ but also presents a general absorption line-shape for organic excitons near their onset from which σ_s and $E_{\mathrm{SE},0}$ can be obtained. To further validate the model, we applied eq. (4) to T-dependent EQE spectra, as demonstrated in **Figure 4b** for neat Y6 and IT-4F. Using neat materials avoids the influences of CT states in the low-energy tail although trap states are always present at lower energies. Doing so, we obtain σ_s values of 47.0±0.7 meV for Y6 and 35.0±2.6 meV for IT-4F (see **Figure S10** in the **Supplementary Information**). More fittings on room temperature EQE spectra of other material systems are shown in the **Figure S11** in the **Supporting Information**).

For blend systems, the full experimental sub-gap EQE can be reconstructed assuming $\alpha(E) = \alpha_{\mathrm{SE}}(E) + \alpha_{\mathrm{CT}}(E) + \alpha_{\mathrm{t}}(E)$ constituting the exponentially decaying absorption coefficient according to eq. 4 and the sum of two Gaussian functions as per eq. 3 (CT states and deep trap states). In **Figure 4b,** we demonstrate the model for PBDB-T:$PC_{70}BM$ using the parameters $E_{\mathrm{SE},0} =$ 1.89 eV and $\sigma_s = 60$ meV, and other Gaussian fit parameters summarized in **Table S1** in the **Supplementary Information**. PBDB-T:$PC_{70}BM$ belongs to the group of blends for which $E_{\mathrm{CT}} \ll E_{\mathrm{SE},0}$ with $\Delta(E_{\mathrm{CT}} - E_{\mathrm{SE},0}) \approx 0.45$ eV. Nevertheless, the simplified model reproduces the strong spectral dependence of the experimental $E_{\mathrm{U}}^{\mathrm{app}}$, including the parabolic behaviour in the SE-dominated regime. On the other hand, by keeping all other parameters constant while increasing E_{CT} with respect to $E_{\mathrm{SE},0}$, the emergence of the $E_{\mathrm{U}}^{\mathrm{app}} = kT$ plateau at around 1.6±0.1 eV can be reproduced.

In the absence of CT states, the above model predicts three sub-gap regimes of $\alpha(E)$ based on the dominant disorder mechanism as illustrated in **Figure 4c**. The steepness close to the gap is determined by σ_{S}, causing a redshift of the effective energy gap and an overall broadening with increasing σ_{S}. Although $E_{\mathrm{U}}^{\mathrm{app}}$ of organic semiconductors does not represent σ_s at any energy, a positive correlation between $E_{\mathrm{U}}^{\mathrm{app}}$ and σ_{S} may be observed at energies close to the absorption onset. This is simulated for the two cases $\sigma_s = 70$ meV and $\sigma_s = 100$ meV as shown in **Figure S9**: For $\sigma_{\mathrm{S}} = 70$ meV, $E_{\mathrm{U}}^{\mathrm{app}}$ reaches kT at $\alpha(E)$ values 3 to 4 orders of magnitudes below α_{sat}, while this is 6 orders below α_{sat} for $\sigma_s =$ 100 meV. For energies well-below the bandgap $E_{\mathrm{U}}^{\mathrm{app}} \approx kT$, which can be considered as the spectral range where σ_{D} dominates, i.e. $\sigma_{\mathrm{D}}(T) = kT$. In our model, the Boltzmann factor stems from the absorption rate that describes the occupation of vibrational modes, in accordance with Marcus theory in the limit of relatively low reorganization energies of the excited state. We note that the equality $E_{\mathrm{U}}(T) = \sigma_{\mathrm{S}} + \sigma_{\mathrm{D}}(T)$ fails in the case of organic semiconductors, because σ_{S} and $\sigma_{\mathrm{D}}(T)$ define the steepness of $\alpha_{\mathrm{SE}}(E)$ at different energies.

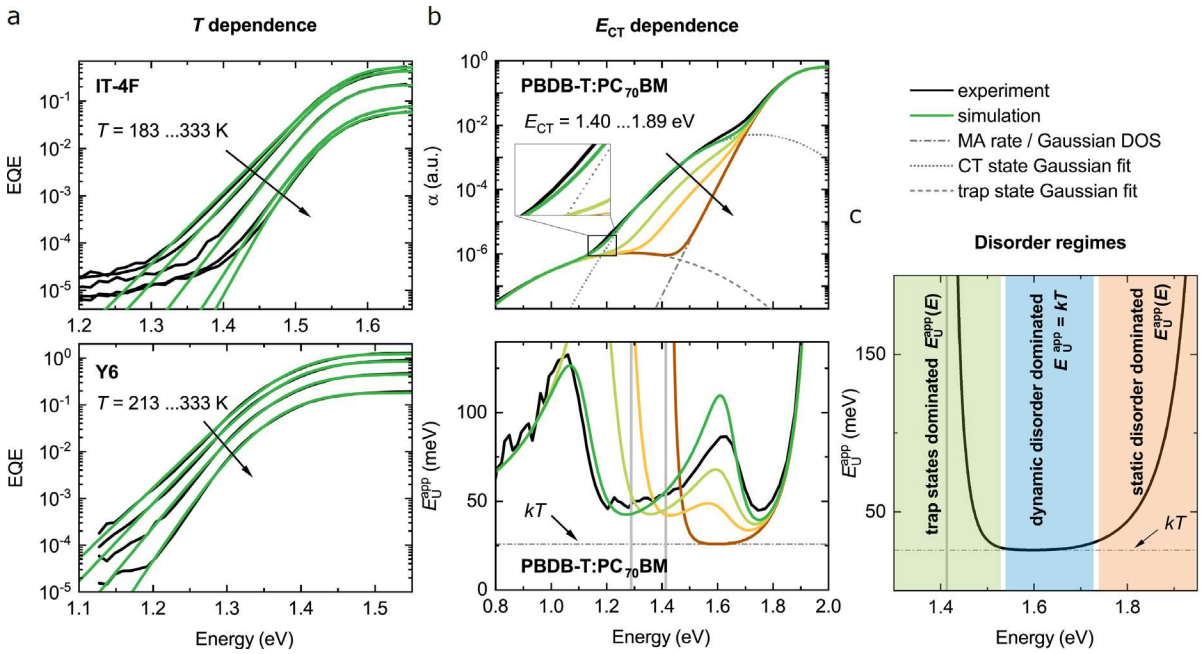

Figure 4 | The sub-bandgap EQE as a function of temperature and charge transfer energy. a, Experimental (black lines) and simulated (green lines) sub-gap EQE spectra of IT-4F and Y6. **b,** The line-shape of the experimental EQE of PBDB-T:PC$_{70}$BM can be described by Gaussian fits corresponding to (i) CT state absorption, (ii) trap state absorption and (iii) the SE absorption coefficient in the spectral range of singlet absorption. In the experiment, $E_{\mathrm{U}}^{\mathrm{app}}$ is above kT, since $E_{\mathrm{CT}} \ll E_{\mathrm{SE},0}$. Increasing E_{CT} in the simulation ($E_{\mathrm{CT}} \rightarrow E_{\mathrm{SE},0}$) results in $E_{\mathrm{U}}^{\mathrm{app}} \rightarrow kT$ between 1.5 to 1.7 eV. **c,** Schematic representation of the spectral regimes of $E_{\mathrm{U}}^{\mathrm{app}}$ dominated by: (i) static disorder close to the band edge, (ii) dynamic disorder where $E_{\mathrm{U}}^{\mathrm{app}} = kT$ and (iii) trap state absorption well-below the gap.

Finally, trap state absorption is typically observed 6 orders of magnitude below α_{sat} limiting the spectral range dominated by σ_{D}. From that and the simulations in Figure S9, we estimate that it is possible to observe $E_{\mathrm{U}}^{\mathrm{app}} \approx kT$ only when $\sigma_s < 100$ meV. Other conditions that must be met are: (i) the neat phase absorption of one component is spectrally separated from the other neat phase absorption, as well as from the CT states and trap states; (ii) the dynamic range of the EQE (or α) measurement is sufficiently wide to measure photocurrent at wavelengths well below the absorption onset of the neat material; and (iii) optical cavity effects are not significant. Exponential sub-gap EQE spectra previously reported in literature for BHJs often do not fulfill these requirements, explaining reported Urbach energies much larger than kT. Importantly, the $E_{\mathrm{U}}^{\mathrm{app}}$ spectra introduced here do not suffer from the short fitting ranges of previous of E_{U} measurements. In contrast, we have shown that an exponential distribution of tail states cannot explain the sub-gap spectral line-shape associated with singlet absorption, nor CT or trap state absorption in organic semiconductors.

Conclusion

In summary, we find that for a large number of organic semiconductors, the sub-gap slope of the excitonic absorption coefficient equals the thermal energy kT within the variations caused by the optical interference. While exponential absorption tails have been previously observed mainly in non-fullerene systems, we show that this property is universal for organic semiconductors and consistent with a Gaussian density of excitonic states undergoing Boltzmann-like thermally activated optical transitions. A theory for the Boltzmann factor representing σ_{D} is presented via the extended Marcus

theory in which the excited state is more delocalised than the ground state. σ_S is shown to arise from the width of the Gaussian DOS and to broaden the absorption onset at energies close to the optical gap. Using our model for the sub-gap excitonic absorption tail, it is possible to discriminate spectral regimes dominated by σ_D and σ_S, as well as to reproduce the temperature dependence of absorption coefficient due to excitons. This modified view of the sub-gap absorption coefficient in disordered organic semiconductors clarifies a longstanding debate concerning the shape of the DOS and the relevance of an Urbach description in these important and intriguing materials.

Methods

Solar cells were fabricated with either a conventional architecture ITO/PEDOT:PSS/active layer/Ca/Al or inverted architecture ITO/ZnO/active layer/MoO_3/Ag. All material acronyms are detailed in the **Supplementary Information**. For a conventional device architecture, 30 nm of PEDOT:PSS was spin-coated at 6000 rpm for 30 s onto precleaned ITO substrates and annealed at 155 °C for 15 minutes. For an inverted device architecture with 30 nm of ZnO, a solution of 200 mg of zinc acetate dihydrate in 2-methoxyethanol (2 ml) and ethanolamine (56 µl) was prepared and stirred overnight under ambient conditions. The ZnO layer formed upon spin-coating the solution at 4000 rpm followed by thermal annealing at 200 °C for 60 minutes. The processing conditions of the individual active layers are discussed in the **Supplementary Information**. For the EQE measurements, a homebuilt setup including a Perkin Elmer UV/VIS/NIR spectrometer (LAMBDA 950) as a source for monochromatic light was used. The light was chopped at 273 Hz and directed onto the device under test (DUT). The resulting photocurrent was amplified by a low noise current amplifier (FEMTO DLPCA-200) and measured with the Stanford SR860 lock-in amplifier. To decrease the noise floor of the setup, the DUT was mounted in an electrically shielded and temperature controlled Linkam sample stage. An integration time up to 1000 seconds was used for detecting wavelengths above 1500 nm. NIST-calibrated silicon and GaAs photodiodes from Newport were used as a calibration reference. The temperature inside the Linkam sample stage was set to -120 to 60 ^{o}C by the Linkam T96 temperature controller in combination with an LNP96 liquid nitrogen pump. The commercial amorphous silicon thin film solar cell, used for temperature dependent EQE measurements, was manufactured by TRONY with the part number sc80125s-8.

Data Availability

The data that support the findings of this study are available from the corresponding author upon reasonable request

References

(1) Zhao, W.; Li, S.; Yao, H.; Zhang, S.; Zhang, Y.; Yang, B.; Hou, J. Molecular Optimization Enables over 13% Efficiency in Organic Solar Cells. *J. Am. Chem. Soc.* **2017**, *139* (21), 7148–7151. https://doi.org/10.1021/jacs.7b02677.

(2) Cui, Y.; Yao, H.; Zhang, J.; Xian, K.; Zhang, T.; Hong, L.; Wang, Y.; Xu, Y.; Ma, K.; An, C.; et al. Single-Junction Organic Photovoltaic Cells with Approaching 18% Efficiency. *Adv. Mater.* **2020**, *32* (19), 1–7. https://doi.org/10.1002/adma.201908205.

(3) Urbach, F. The Long-Wavelength Edge of Photographic Sensitivity and of the Electronic Absorption of Solids. *Phys. Rev.* **1953**, *92* (5), 1324. https://doi.org/10.1103/PhysRev.92.1324.

(4) Cody, G. D.; Tiedje, T.; Abeles, B.; Brooks, B.; Goldstein, Y. Disorder and the Optical-Absorption Edge of Hydrogenated Amorphous Silicon. *Phys. Rev. Lett.* **1981**, *47* (20), 1480–

1483. https://doi.org/10.1103/PhysRevLett.47.1480.

(5) Bonalde, I.; Medina, E.; Rodríguez, M.; Wasim, S. M.; Marín, G.; Rincón, C.; Rincón, A.; Torres, C. Urbach Tail, Disorder, and Localized Modes in Ternary Semiconductors. *Phys. Rev. B - Condens. Matter Mater. Phys.* **2004**, *69* (19), 1–5. https://doi.org/10.1103/PhysRevB.69.195201.

(6) Bansal, B.; Dixit, V. K.; Venkataraman, V.; Bhat, H. L. Alloying Induced Degradation of the Absorption Edge of in As XSb1-X. *Appl. Phys. Lett.* **2007**, *90* (10). https://doi.org/10.1063/1.2711388.

(7) Pankove, J. I. Absorption Edge of Impure Gallium Arsenide. *Phys. Rev.* **1965**, *140* (6A). https://doi.org/10.1103/PhysRev.140.A2059.

(8) Kurik, M. V. Urbach Rule. *Phys. Status Solidi* **1971**, *8* (1), 9–45. https://doi.org/10.1002/pssa.2210080102.

(9) Grein, C. H.; John, S. Temperature Dependence of the Urbach Optical Absorption Edge: A Theory of Multiple Phonon Absorption and Emission Sidebands. *Phys. Rev. B* **1989**, *39* (2), 1140–1151. https://doi.org/10.1103/PhysRevB.39.1140.

(10) Corkish, R.; Green, M. A. Band Edge Optical Absorption in Intrinsic Silicon: Assessment of the Indirect Transition and Disorder Models (Journal of Applied Physics (1993) 73 (3988)). *J. Appl. Phys.* **1993**, *74* (10), 6462. https://doi.org/10.1063/1.355344.

(11) Dow, J. D.; Redfield, D. Toward a Unified Theory of Urbach's Rule and Exponential Absorption Edges. *Phys. Rev. B* **1972**, *5* (2), 594–610. https://doi.org/10.1017/CBO9781107415324.004.

(12) Vandewal, K.; Tvingstedt, K.; Gadisa, A.; Inganäs, O.; Manca, J. V. Relating the Open-Circuit Voltage to Interface Molecular Properties of Donor:Acceptor Bulk Heterojunction Solar Cells. *Phys. Rev. B - Condens. Matter Mater. Phys.* **2010**, *81* (12), 1–8. https://doi.org/10.1103/PhysRevB.81.125204.

(13) Rahimi, K.; Botiz, I.; Agumba, J. O.; Motamen, S.; Stingelin, N.; Reiter, G. Light Absorption of Poly(3-Hexylthiophene) Single Crystals. *RSC Adv.* **2014**, *4* (22), 11121–11123. https://doi.org/10.1039/c3ra47064d.

(14) Zarrabi, N.; Sandberg, O. J.; Zeiske, S.; Li, W.; Riley, D. B.; Meredith, P.; Armin, A. Charge-Generating Mid-Gap Trap States Define the Thermodynamic Limit of Organic Photovoltaic Devices. *Nat. Commun.* **2020**, *in press*.

(15) Benduhn, J.; Tvingstedt, K.; Piersimoni, F.; Ullbrich, S.; Fan, Y.; Tropiano, M.; McGarry, K. A.; Zeika, O.; Riede, M. K.; Douglas, C. J.; et al. Intrinsic Non-Radiative Voltage Losses in Fullerene-Based Organic Solar Cells. *Nat. Energy* **2017**, *2* (April), 17053. https://doi.org/10.1038/nenergy.2017.53.

(16) Qian, D.; Zheng, Z.; Yao, H.; Tress, W.; Hopper, T. R.; Chen, S.; Li, S.; Liu, J.; Chen, S.; Zhang, J.; et al. Design Rules for Minimizing Voltage Losses in High-Efficiency Organic Solar Cells. *Nat. Mater.* **2018**, *17* (8), 703–709. https://doi.org/10.1038/s41563-018-0128-z.

(17) Ran, N. A.; Love, J. A.; Takacs, C. J.; Sadhanala, A.; Beavers, J. K.; Collins, S. D.; Huang, Y.; Wang, M.; Friend, R. H.; Bazan, G. C.; et al. Harvesting the Full Potential of Photons with Organic Solar Cells. *Adv. Mater.* **2016**, *28* (7), 1482–1488. https://doi.org/10.1002/adma.201504417.

(18) Liu, S.; Yuan, J.; Deng, W.; Luo, M.; Xie, Y.; Liang, Q.; Zou, Y. High-Efficiency Organic Solar Cells with Low Non-Radiative Recombination Loss and Low Energetic Disorder. *Nat. Photonics*

2020, *in press*. https://doi.org/10.1038/s41566-019-0573-5.

(19) Jain, N.; Chandrasekaran, N.; Sadhanala, A.; Friend, R. H.; McNeill, C. R.; Kabra, D. Interfacial Disorder in Efficient Polymer Solar Cells: The Impact of Donor Molecular Structure and Solvent Additives. *J. Mater. Chem. A* **2017**, *5* (47), 24749–24757. https://doi.org/10.1039/c7ta07924a.

(20) Bässler, H. Charge Transport in Disordered Organic Photoconductors a Monte Carlo Simulation Study. *Phys. Status Solidi* **1993**, *175* (1), 15–56. https://doi.org/10.1002/pssb.2221750102.

(21) Beenken, W. J. D.; Herrmann, F.; Presselt, M.; Hoppe, H.; Shokhovets, S.; Gobsch, G.; Runge, E. Sub-Bandgap Absorption in Organic Solar Cells: Experiment and Theory. *Phys. Chem. Chem. Phys.* **2013**, *15* (39), 16494–16502. https://doi.org/10.1039/c3cp42236d.

(22) Blakesley, J. C.; Neher, D. Relationship between Energetic Disorder and Open-Circuit Voltage in Bulk Heterojunction Organic Solar Cells. *Phys. Rev. B - Condens. Matter Mater. Phys.* **2011**, *84* (7). https://doi.org/10.1103/PhysRevB.84.075210.

(23) Kaiser, C.; Zeiske, S.; Meredith, P.; Armin, A. Determining Ultralow Absorption Coefficients of Organic Semiconductors from the Sub-Bandgap Photovoltaic External Quantum Efficiency. *Adv. Opt. Mater.* **2019**, *8* (1), 1901542. https://doi.org/https://doi.org/10.1002/adom.201901542.

(24) Armin, A.; Zarrabi, N.; Sandberg, O. J.; Kaiser, C.; Zeiske, S.; Li, W.; Meredith, P. Limitations of Charge Transfer State Parametrisation and Relevance for Non-Fullerene Acceptors. *Adv. Energy Mater.* **2020**, *in press*. https://doi.org/10.1002/aenm202001828.

(25) Leblanc, F. Related Content Accurate Determination of the Urbach Energy of A- Si : H Thin Films by Correction for the Interference Effect. *Japanese J. Appl. Phys. Jpn. J. Appl. Phys* **1994**, *33*, 1755–1758. https://doi.org/10.1143/jjap.33.l1755.

(26) Sandberg, O. J.; Zeiske, S.; Zarrabi, N.; Meredith, P.; Armin, A. Charge Carrier Transport and Generation via Trap-Mediated Optical Release in Organic Semiconductor Devices. *Phys. Rev. Lett.* **2020**, *124* (12), 128001. https://doi.org/10.1103/PhysRevLett.124.128001.

(27) Gielen, S.; Kaiser, C.; Verstraeten, F.; Kublitski, J.; Benduhn, J.; Spoltore, D.; Verstappen, P.; Maes, W.; Meredith, P.; Armin, A.; et al. Intrinsic Detectivity Limits of Organic Near-Infrared Photodetectors. *Adv. Mater.* **2020**, *in press*. https://doi.org/DOI: 10.1002/adma.202003818.

(28) Nikolis, V. C.; Mischok, A.; Siegmund, B.; Kublitski, J.; Jia, X.; Benduhn, J.; Hörmann, U.; Neher, D.; Gather, M. C.; Spoltore, D.; et al. Strong Light-Matter Coupling for Reduced Photon Energy Losses in Organic Photovoltaics. *Nat. Commun.* **2019**, *10* (1), 1–8. https://doi.org/10.1038/s41467-019-11717-5.

(29) Searle, T. M.; Jackson, W. A. Static versus Electron-Phonon Disorder in Amorphous Si: H and Its Alloys. *Philos. Mag. B Phys. Condens. Matter; Stat. Mech. Electron. Opt. Magn. Prop.* **1989**, *60* (2), 237–255. https://doi.org/10.1080/13642818908211192.

(30) Cody, G. D. Urbach Edge of Crystalline and Amorphous Silicon: A Personal Review. *J. Non. Cryst. Solids* **1992**, *141* (C), 3–15. https://doi.org/10.1016/S0022-3093(05)80513-7.

(31) Tang, J. Electron-Transfer Reactions Involving Non-Linear Spin-Boson Interactions. *Chem. Phys.* **1994**, *188* (2–3), 143–160. https://doi.org/10.1016/0301-0104(94)00254-1.

(32) Casado-pascual, J.; Morillo, M.; Goychuk, I.; Hänggi, P.; Morillo, M. The Role of Different Reorganization Energies within the Zusman Theory of Electron Transfer The Role of Different

Reorganization Energies within the Zusman Theory of Electron Transfer. *J. Chem. Phys.* **2003**, *118* (1), 291. https://doi.org/10.1063/1.1525799.

(33) Keil, T. H. Theory of the Urbach Rule. *Phys. Rev.* **1966**, *144* (2), 582–587. https://doi.org/10.1103/PhysRev.144.582.

(34) Hood, S.; Zarrabi, N.; Meredith, P.; Kassal, I.; Armin, A. Measuring Energetic Disorder in Organic Semiconductors Using the Photogenerated Charge-Separation Efficiency. *J. Phys. Chem. Lett.* **2019**, *10* (14), 3863–3870. https://doi.org/10.1021/acs.jpclett.9b01304.

(35) Miller, A.; Abrahams, E. Impurity Conduction at Low Concentrations. *Phys. Rev.* **1960**, *120* (3), 745–755. https://doi.org/10.1103/PhysRev.120.745.

Acknowledgements

This work was funded through the Welsh Government's Sêr Cymru II Program 'Sustainable Advanced Materials' (Welsh European Funding Office − European Regional Development Fund). C.K. is recipient of a UKRI EPSRC Doctoral Training Program studentship. N.Z. is funded by a studentship through the Sêr Cymru II Program. P.M. is a Sêr Cymru II Research Chair and A.A. is a Rising Star Fellow also funded through the Welsh Government's Sêr Cymru II 'Sustainable Advanced Materials' Program (European Regional Development Fund, Welsh European Funding Office and Swansea University Strategic Initiative).

Author Contributions

AA and PM provided the overall leadership of the project. OJS and AA conceptualised the idea. CK and AA designed the experiments. CK performed most measurements, analysed the data, performed optical modelling and drafted the manuscript. OJS developed the theoretical model. CK, OJS and AA interpreted the data. NZ assisted with $\mathrm{EQE_{PV}}$ measurements. WL fabricated the devices. All co-authors contributed in the development of the manuscript which was initially drafted by CK.

Additional information

Supplementary Information

Competing interests: The authors declare no competing interests.

Figures

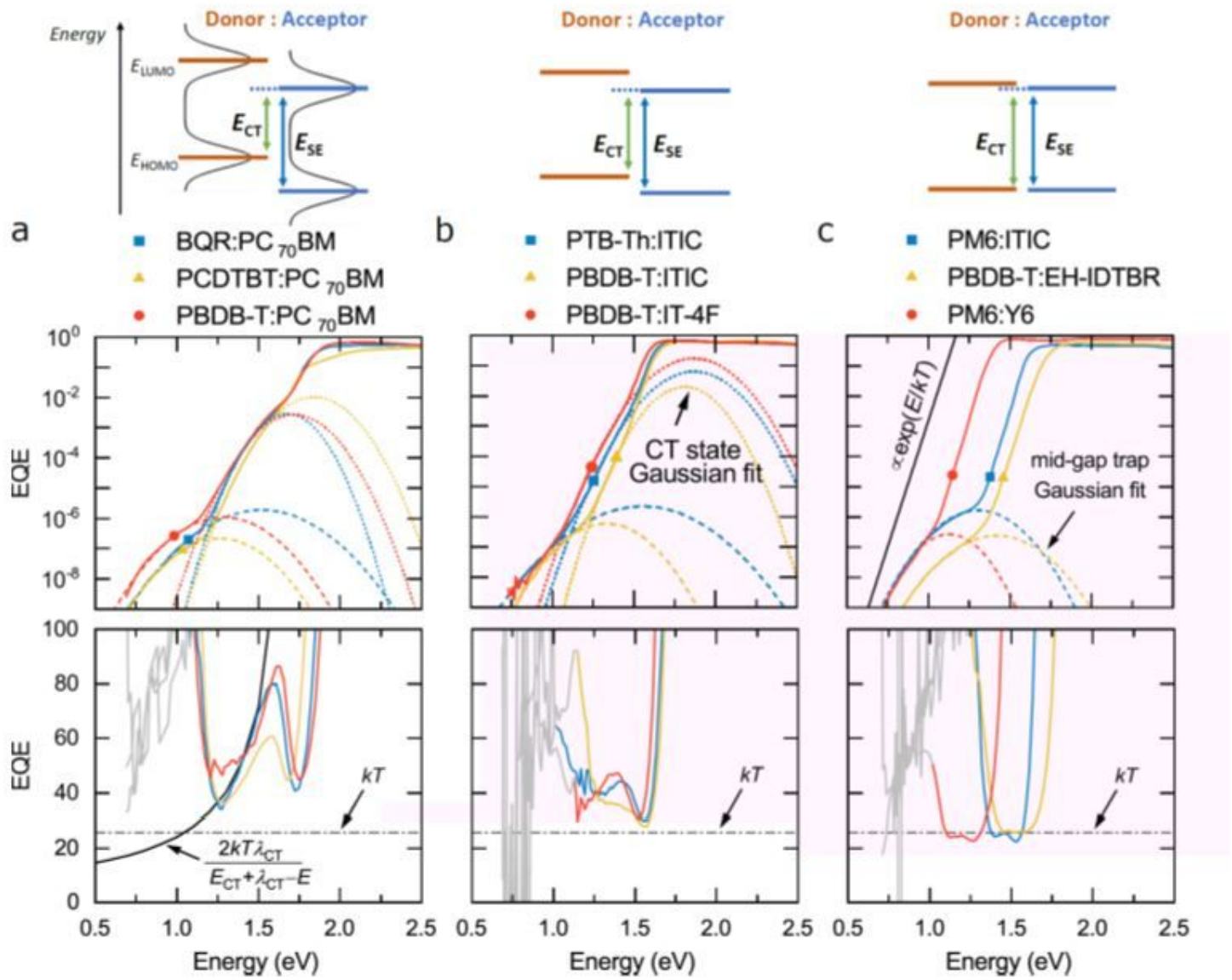

Figure 1

EQE and E_U^app for organic BHJs with different energetic offsets between the HOMO energy levels of donor and acceptor. From Gaussian fits in the spectral range of charge transfer state and trap state absorption, the charge transfer energy (E_CT) and trap energy (E_t) are extracted where possible. For low-energy offset materials, such as PM6:Y6, PM6:ITIC and PBDB-T:EH-IDTBR, the EQE tail has the form e^(E/kT) and E_U^app roughly equals kT in the spectral range that is dominated by the absorption of the acceptor. For large-offset material systems, such as BQR:PC70BM, PBDB-T:PC70BM and PCDTBT:PC70BM, E_U^app shows a 2kTλ_CT/(E_CT+λ_CT-E) dependence in the spectral range of CT absorption.

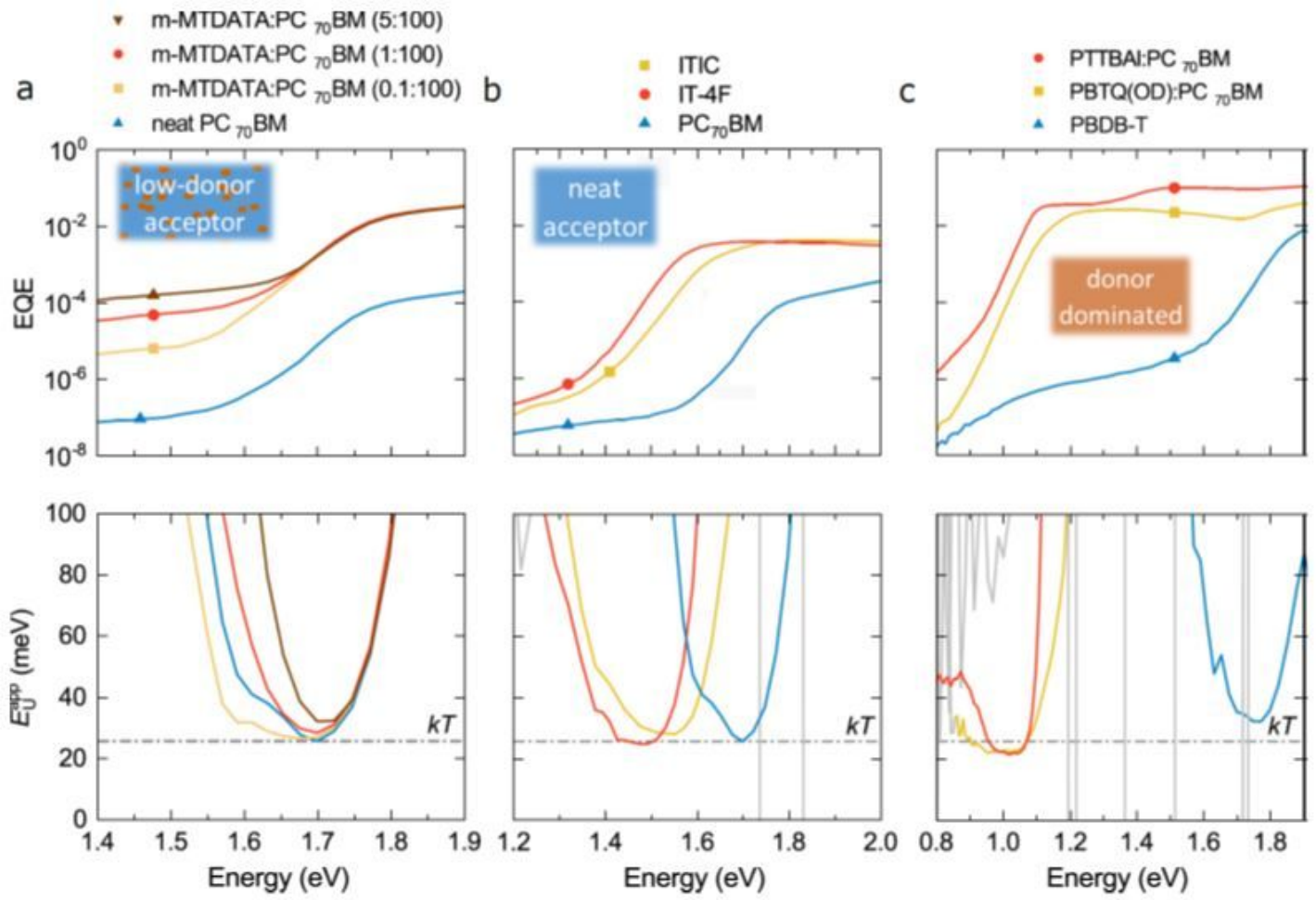

Figure 2

EQE tail dominated by neat material absorption. a, The inverse slope of the logarithm of the EQE for a series of m-MTDATA sensitized PC70BM solar cells. The widest energy range over which E_U^app equals kT is observed for 0.1 mol% m-MTDATA in PC70BM due to improved exciton dissociation in comparison to neat PC70BM. BHJ examples for which the EQE tail is partially dominated by b, the neat donor absorption or by c, the neat acceptor absorption hence showing E_U^app≈kT in some parts of the spectrum. EQE spectra of PTTBAI:PC70BM and PBTQ(OD):PC70BM are taken from reference 27.

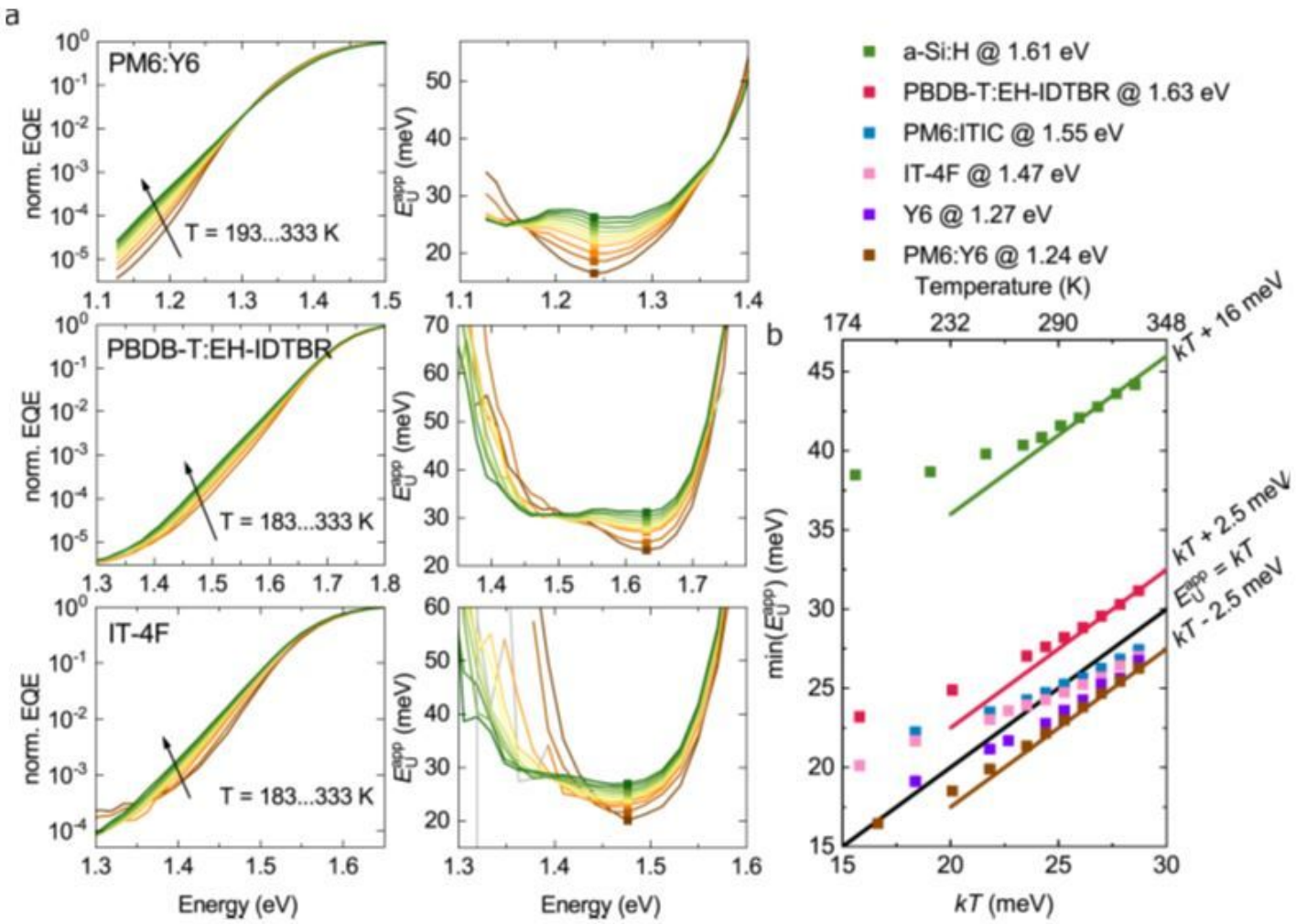

Figure 3

Temperature dependent apparent Urbach energies. a, Normalized sub-gap EQE and Urbach energy (E_U^app) spectra of inverted PM6:Y6, PBDB-T:EH-IDTBR and neat IT-4F solar cells at different temperatures. Independent of temperature, E_U^app spectra show a local minimum (solid markers) at a constant energy within the spectral range dominated by exciton absorption. b, Minimum E_U^app as a function of kT for all tested materials systems including a commercial a-Si:H thin-film solar cell.

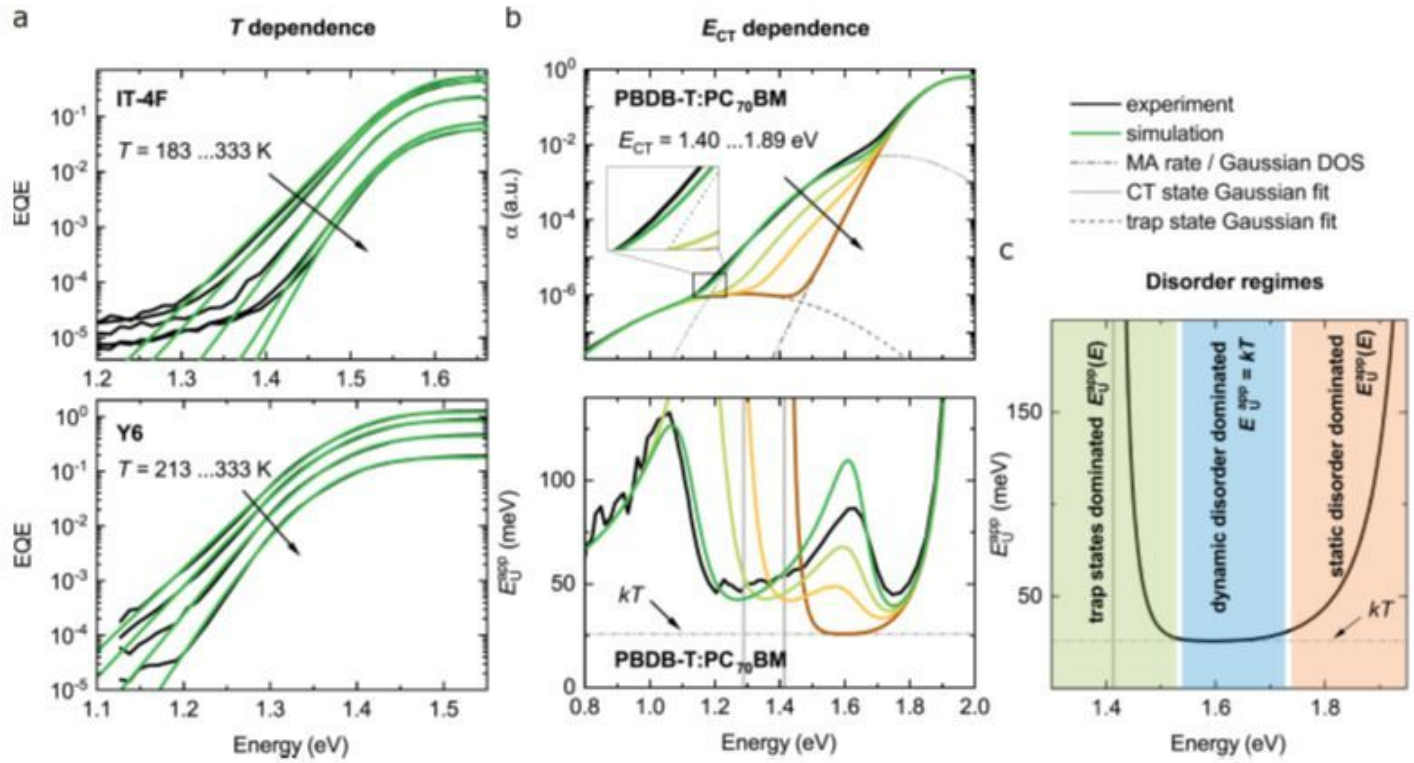

Figure 4

The sub-bandgap EQE as a function of temperature and charge transfer energy. a, Experimental (black lines) and simulated (green lines) sub-gap EQE spectra of IT-4F and Y6. b, The line-shape of the experimental EQE of PBDB-T:PC70BM can be described by Gaussian fits corresponding to (i) CT state absorption, (ii) trap state absorption and (iii) the SE absorption coefficient in the spectral range of singlet absorption. In the experiment, E_U^app is above kT, since E_CT≫E_(SE,0). Increasing E_CT in the simulation (E_CT≈E_(SE,0)) results in E_U^app≈kT between 1.5 to 1.7 eV. c, Schematic representation of the spectral regimes of E_U^app dominated by: (i) static disorder close to the band edge, (ii) dynamic disorder where E_U^app=kT and (iii) trap state absorption well-below the gap.

Supplementary Files

This is a list of supplementary files associated with this preprint. Click to download.

- SupplementaryInfoUrbachNaturePhotonicsSubmitted.docx